Bulletin of the Seismological Society of America, Vol. 101, No. 5, pp. 2153–2161, October 2011, doi: 10.1785/0120100258

Estimation of the Depth of Anisotropy Using Spatial Coherency of Shear-Wave Splitting Parameters

by Kelly H. Liu and Stephen S. Gao

Abstract Shear-wave splitting (SWS) analyses are essential in understanding the structure and dynamics of the Earth's deep interior. While splitting measurements have excellent horizontal resolution relative to other anisotropy-measuring techniques, their vertical resolution is low due to the steep incidence angle of the seismic phases used by the analyses. Here, using synthetic and real data, we present and test a simple approach to estimate the optimal depth of anisotropy by measuring the spatial coherency of the splitting parameters. The approach searches for the optimal depth by computing a spatial variation factor. Tests using synthetic SWS data produced with varying number of events, number of stations, and levels of noise suggest that the approach can satisfactorily find the depth of the source of anisotropy. Successful application of the depth-estimation procedure requires well-defined splitting parameters obtained from a multistation network and multiple events from a decent back-azimuthal range. It also requires significant and smooth spatial variations of anisotropy with horizontal axis of symmetry within a single layer of anisotropy. We applied the approach to 448 pairs of splitting measurements obtained at about 50 stations on the Ethiopian Plateau and found an optimal depth of anisotropy of about 300 km, suggesting an asthenospheric origin of the observed anisotropy.

Introduction

Shear-wave splitting (SWS) analysis using teleseismic *SKS*, *SKKS*, and *PKS* phases (hereafter referred collectively as *XKS*) is one of the most widely-used techniques in earthquake seismology. Over the past 30 years, hundreds of *XKS*-splitting studies have played a unique role in the detection of mantle fabrics and in the understanding of mantle dynamic processes that formed the fabrics (see reviews by Silver [1996], Savage [1999], and Wustefeld *et al.* [2009] for partial lists of SWS studies). Because of the steep incidence of the *XKS* ray paths, *XKS*-splitting observations have good lateral resolution (relative to other anisotropy-measuring techniques) but low vertical resolution.

The most commonly-used approach to estimate the depth (which is defined as that of the center of the anisotropic layer) of a horizontal anisotropic slab responsible for the observed SWS is the intersecting Fresnel-zone approach (Alsina and Snieder, 1995). Because of the finite frequencies of the *XKS* waveform, the ray can be treated as a tube defined by its first Fresnel zone (Alsina and Snieder, 1995) approximately centered at the geometric ray path. The diameter of the tube increases with the dominant period and depth. The splitting parameters reflect the combined effect of seismic anisotropy inside the tube. Alsina and Snieder (1995) proposed that if two *XKS* events from opposite directions have different splitting parameters (fast direction ϕ and splitting time δt) at the same station, the anisotropic layer must reside below the depth at which the two tubes intersect. Similarly, if an *XKS* event produces different splitting parameters at two stations, the layer must be shallower than the depth at which the two tubes intersect. Clearly, among other limitations, the Alsina and Snieder (1995) approach is limited to situations in which events from opposite directions are available, and significant lateral variations in seismic anisotropy exist between nearby stations.

In this report, we provide a modified (circular rather than linear statistics) version of an approach that Gao *et al.* (2010) recently proposed to estimate the depth of anisotropy using the spatial coherency of splitting parameters. We then test it using synthetic and real data sets and discuss its dependence on various parameters such as network density, number of available *XKS* events, azimuthal distribution of the events, and quality of *XKS* measurements. Similar to the widely used approach proposed by Alsina and Snieder (1995), our approach is applicable to the most common assumption when the vast majority of shear-wave splitting measurements were interpreted in previous studies; that is, the observed shear-wave splitting is from a single horizontal layer of anisotropy with hexagonal symmetry and a horizontal symmetry axis. Our approach is based on the Fresnel-zone principle and thus can be considered as a more generalized

and quantitative extension of the Alsina and Snieder (1995) approach.

Variation of Spatial Coherency as a Function of Assumed Depths of Anisotropy

Because most *XKS* waves have a nonvertical angle of incidence, for a layer of anisotropy at a given depth, the area sampled by the tube varies as a function of the back azimuth, epicentral distance, and focal depth of the event. In this section, we use a regularly spaced synthetic seismic network and two seismic events from opposite directions to visually demonstrate such dependence. More realistic network and azimuthal configurations will be used in the following sections.

The synthetic network consists of 49 stations with 1° spacing in an area centered near the equator (Fig. 1). The stations recorded *SKS* waves from two surface events, one from the north with an epicentral distance of 100° to the center of the network and another from the south with the same epicentral distance. In the model, the center of a horizontal, vertically homogeneous anisotropic layer is placed at 200 km depth. The fast direction at a given point within the layer is given by

$$\phi(r) = \phi_0 + c_1 r, \tag{1}$$

and the splitting time is given by

$$\delta t(r) = \delta t_0 + c_2 \exp(-c_3 R^2), \tag{2}$$

where r is the distance (in degrees) between the point and the lower-left corner of the area shown in Figure 1 (point $[-5, -5]$); R is the distance (in degrees) between the point and point (0,0), which is approximately the center of the network; and c_1, c_2, and c_3 are constants. The following parameters are used to produce the measurements in Figure 1 and for all the synthetic tests presented in the study: $\phi_0 = 0°$, $\delta t_0 = 0.5$ s, $c_1 = 10$, $c_2 = 1.5$, and $c_3 = 0.2$. These parameters result in linearly varying ϕ values with regard to r in the range of 0–140.2° and exponentially decaying δt values from point (0,0) with a range of 0.5–2.0 s (Fig. 1). The magnitudes of the spatial variations resemble those of most regional studies. Note that the choice of the functions (equations 1

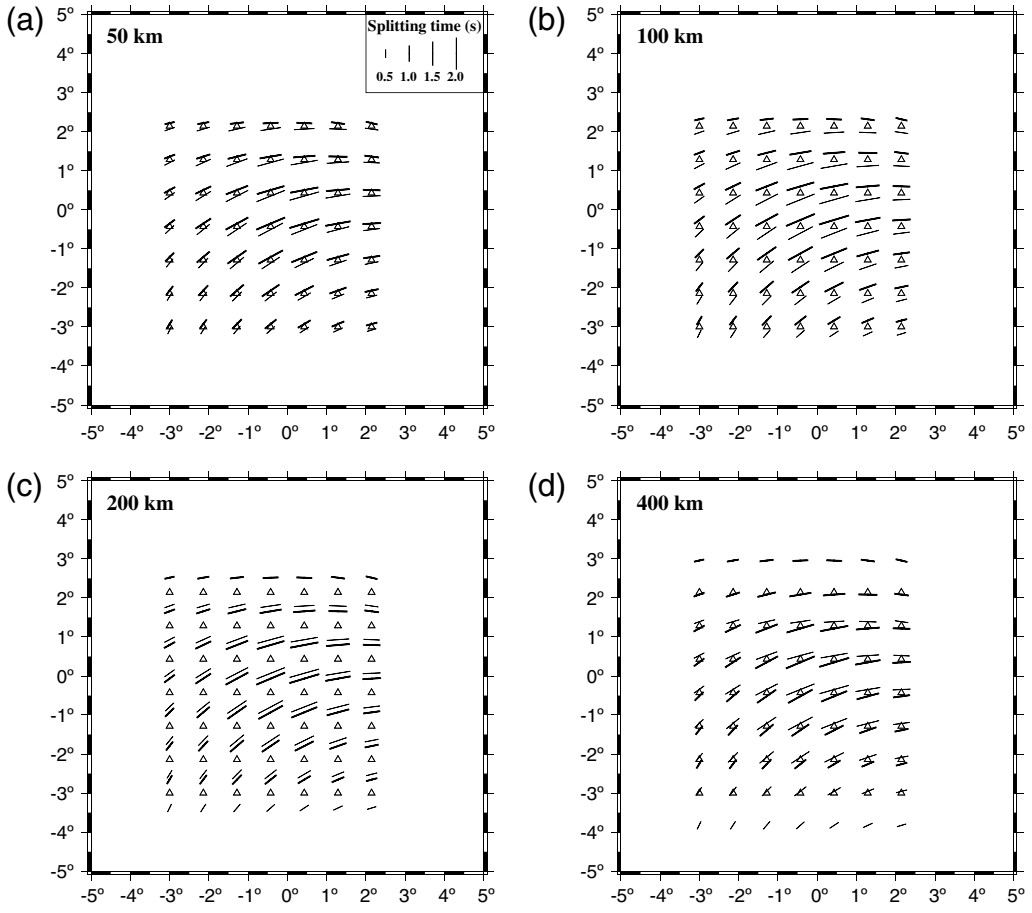

Figure 1. Synthetic shear-wave splitting parameters from 49 stations (triangles) plotted above the ray-piercing points at various depths. The direction of the bars represents the fast polarization direction, and the length is proportional to the splitting time. Thick bars are splitting parameters from an event from the north, and thin bars are those from the south. Note the spatial coherency for both ϕ and δt at the depth of 200 km (c),which is the depth of the anisotropic layer used to generate the splitting parameters.

and 2) and the parameters in the functions is largely arbitrary. Numerous functions and parameters can be used, as long as they produce significant and smooth variations of ϕ and δt across the study area.

We next compute the geographic coordinates of each of the ray-piercing points at the center of the anisotropic layer (200-km deep) using the IASP91 Earth model (Kennett and Engdahl, 1991) and calculate the mean splitting parameters inside the first Fresnel zone for which the size is similar to that of the sensitivity kernel that has an approximate diameter of $85 + 0.2D_a$ km, where D_a is the depth of the center of the anisotropic layer, for shear waves with a period of 8 s (which is the dominant period for most *XKS* waves; Favier and Chevrot, 2003). Note that the preceding relation between depth and the size of the kernel was derived empirically from figure 11 of Favier and Chevrot (2003). While not all the points inside the first Fresnel zone contribute equally to the observed anisotropy (Chevrot, 2006), the mean splitting parameters inside the tube are close approximations of the measured splitting parameters for a given ray path, especially for a horizontal slab with vertically homogeneous and horizontally slow-varying anisotropy.

An alternative way to produce synthetic shear-wave splitting measurements for testing the depth-measuring procedure is to create precise synthetic seismograms using a realistic anisotropic Earth model with local spatial variations and to measure splitting parameters using the synthetic seismograms. However, such an approach is not suitable for the main objective of the present study (i.e., testing a technique for estimating the depth of a layer of anisotropy). The main reason for this is that errors will be unavoidably introduced during the generation of synthetic seismograms and when the splitting parameters are measured. Comparative studies (e.g., Vecsey *et al.*, 2008) show that different measuring techniques can lead to significantly different splitting parameters. In addition, data processing parameters such as frequency bands used for filtering and the *XKS* time window selected for the measurements can also lead to different splitting parameters. While the effects of these splitting-measuring techniques and parameters were evaluated in previous studies and deserve additional evaluations, they are beyond the scope of the present study. On the contrary, for testing the depth-estimating procedure proposed here, we need a set of splitting parameters that are free of errors associated with the generation of synthetic seismograms and with the measuring of splitting parameters.

To facilitate the calculation of the mean splitting parameters inside the tube, we produce a discrete database of splitting parameters at densely spaced (0.05° apart) points based on equations (1) and (2). For a given ray path, the splitting time is calculated as the simple mean over the splitting times of the n points inside the tube. Because the fast directions are bidirectional (i.e., axial) data, the mean of the n points inside the tube can be more properly obtained (than simple averaging) using well-established statistical approaches for bidirectional data (Fisher, 1993; Davis, 2002; Gerst and Savage, 2004). First, we compute s and c, which are defined as $s = 1/n \sum_{i=1}^{n} \sin(2\phi_i)$ and $c = 1/n \sum_{i=1}^{n} \cos(2\phi_i)$, where ϕ_i is the fast direction of the i-th point inside the tube. The mean fast direction inside the tube is then computed using

$$\begin{aligned} &0.5 \arctan(s/c), s \geq 0, c \geq 0; \\ &0.5[\arctan(s/c) + 180°], c < 0; \\ &0.5[\arctan(s/c) + 360°], s < 0, c > 0. \end{aligned} \tag{3}$$

The resulting mean splitting parameters (Fig. 1) show a high degree of spatial coherence when downward projected to the ray-piecing points at the true depth of the anisotropy (200 km). There, the Fresnel zones of the ray tubes associated with the two events exhibit maximum overlap (Fig. 1c). On the other hand, when the measurements are placed at the ray-piercing points computed using incorrect depths, the spatial coherency reduces (Fig. 1a,b,d). Obviously, a smaller difference between the assumed and the true depths leads to a smaller distance between the computed and true ray-piercing points and, consequently, results in a greater spatial coherency. Therefore, spatial coherency of observed splitting parameters can be used to estimate the depth of anisotropy beneath an area.

The Depth-Estimating Procedure

In this section, we present a modified version of a procedure proposed by Gao *et al.* (2010) to quantify the dependence of the spatial coherency on assumed depth of anisotropy. The procedure starts with computing the geographic distribution of the ray-piercing points at a series of assumed depths of anisotropy ranging from the surface to the maximum possible depth of anisotropy, based on the IASP91 Earth model (Kennett and Engdahl, 1991). For the synthetic tests in this study, the depth range is 0–400 km, and the incremental interval for the assumed depths is 5 km. For each depth, the study area is divided into overlapping blocks with an area of $Dx \times Dx$ square-degrees. Unless explicitly mentioned, $Dx = 0.1°$ and a distance of 0.05° between the center of neighboring blocks are used for the synthetic and real data tests. The variation factors at this depth, $F_{\delta t}$ for δt and F_{ϕ} for ϕ, are then calculated using

$$F_{\delta t} = \frac{1}{N} \sum_{i=1}^{N} \sqrt{\frac{1}{M_i - 1} \sum_{j=1}^{M_i} (\delta t_{ij} - \overline{\delta t_i})^2} \tag{4}$$

and

$$F_{\phi} = \frac{1}{N} \sum_{i=1}^{N} \sqrt{-\frac{1}{2} \ln(R_i)}, \tag{5}$$

where

$$R_i^2 = \left[\frac{1}{M_i}\sum_{j=1}^{M_i}\cos(2\phi_{ij})\right]^2 + \left[\frac{1}{M_i}\sum_{j=1}^{M_i}\sin(2\phi_{ij})\right]^2, \quad (6)$$

N is the number of blocks, M_i is the number of measurements for the i-th block, ϕ_{ij} and δt_{ij} are the j-th fast direction and splitting delay-time measurement in the i-th block, and $\overline{\delta t_i}$ is the average δt over all the measurements in block i. $F_{\delta t}$ is the mean simple standard deviation (STD), and F_ϕ is the mean circular STD (Fisher, 1993) over all the blocks. When the ϕ observations used for computing the STD in a block span a small (e.g., $\leq 15°$) range, circular (equation 5) and linear (Gao *et al.*, 2010) STDs are similar. The difference increases with the range of ϕ, and thus it is more appropriate to use circular STDs. Note that for the synthetic data set and most well-determined observed splitting parameters, highly similar splitting parameters inside the $Dx \times Dx$ blocks are expected, and thus results from the linear and circular STDs are similar. Indeed, such slow spatial variation in splitting parameters is one of the requirements for the reliable application of the depth-estimating procedure.

The variation factor, F_v, is computed as a dimensionless weighted average of F_ϕ and $F_{\delta t}$; that is,

$$F_v = w_\phi F_\phi + w_{\delta t} F_{\delta t}, \quad (7)$$

where w_ϕ and $w_{\delta t}$ are the weighting factor for the ϕ and δt measurements, respectively.

Because the ϕ measurements have a maximum range of variation of 180° and the δt measurements have a range of about 2.0 s for most studies, we use $w_\phi = 1/180$ degree^{-1} and $w_{\delta t} = 1/2$ s^{-1} so that the variation factors of the two parameters can be combined. Note that if the ϕ (δt) measurements are better determined and/or have a more significant spatial variation than the $\delta t(\phi)$ measurements, increasing $w_\phi(w_{\delta t})$ can lead to more reliably determined depth. The uncertainty in F_v for a given depth is computed as the standard deviation over all the blocks. For the purpose of comparing results from different sets of synthetic parameters, the F_v values are normalized by that at zero depth. Obviously, the optimal depth of the anisotropic layer corresponds to the minimum F_v.

Synthetic Tests

The seismic network used to test the procedure described in the previous section consists of N_{st} stations with a nominal station interval of $\Delta_p = 6°/\sqrt{N_{st}}$. The station on the southwestern corner is located at $(-3°, -3°)$. To resemble irregularities in station spacing, we randomly vary the station coordinates by a maximum of 25% of the amount of station interval; that is, $P = P_0 + 0.5\Delta_p\gamma$, where P_0 is the regularly gridded station latitude or longitude, Δ_p is the nominal station interval, and γ is a random number between -0.5 and 0.5, generated using the *ran4* subroutine in Press *et al.* (1992). N_{ev} earthquakes with epicentral distances randomly distributed in the range of 85°–150° are also generated using the same subroutine (Fig. 2). The spatial distribution of the anisotropic parameters is given by equations (1) and (2).

In this study only the *SKS* phase is used. Because *PKS* and *SKKS* have similar ray parameters to *SKS*, similar results will be obtained if they are used in combination with *SKS* or used separately. For each *SKS* ray path, we compute the coordinates of the ray-piercing point at the assumed depth of the anisotropic layer (i.e., 200 km) and compute the mean splitting parameters within the first Fresnel zone centered at the ray-piercing point. The results, shown in Figure 3, are plotted at four assumed depths. The depth-estimation procedure described in the previous section (The Depth-Estimating Procedure) is then applied to the synthetic data set. The resulting depth variation of F_v, shown in Figure 4, is computed using $N_{st} = 100$ and $N_{ev} = 20$. A well-defined minimum at the true depth (200 km) is found.

To demonstrate that the procedure works well for situations with poor azimuthal coverage, we limit the back azimuths of the 20 events in the ranges of $-90°$ to 90° and 90° to 270°. A clear minimum is also observed on each of the resulting depth-variation curves of F_v (Fig. 5). As the number of stations and/or events is reduced, the region on the F_v curve surrounding the expected minimum broadens (Figs. 6 and 7), resulting in larger uncertainties in the resulting optimal depth.

In order to test the effects of uncertainties of the SWS measurements on the accuracy of the estimated depth of anisotropy, we add random noise to the synthetic splitting parameters before applying the procedure. The added noise

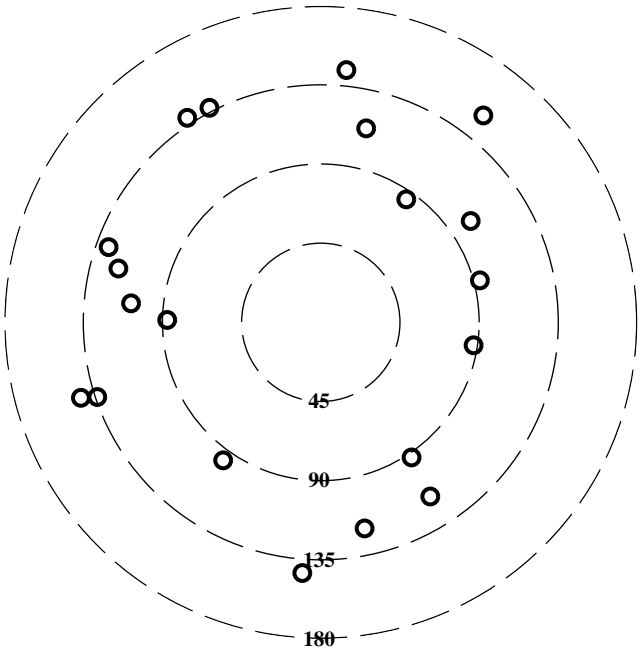

Figure 2. Distribution of events used to generate synthetic splitting parameters shown in Figure 3. Numerals indicate epicentral distances (in degrees) from the center of the imaginary seismic network (Fig. 1).

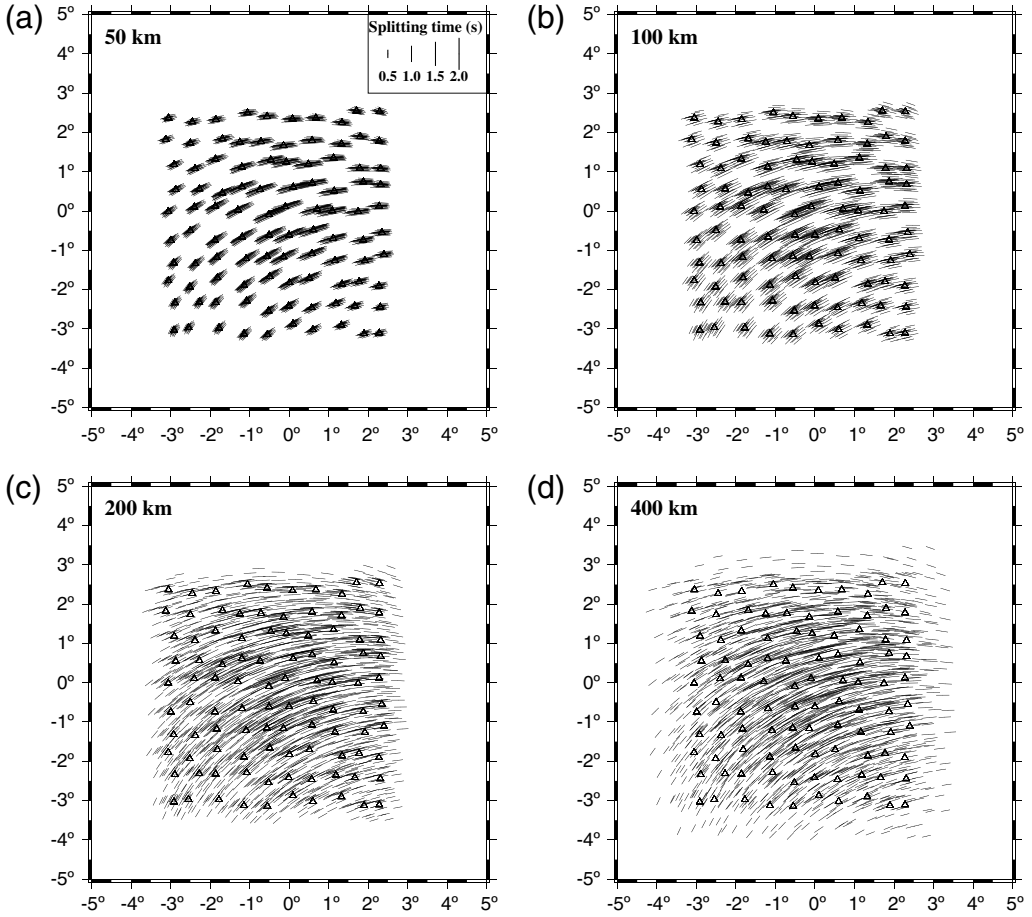

Figure 3. Same as in Figure 1 but for 100 stations and the 20 events shown in Figure 2.

is computed using $2E_\phi\gamma$, where E_ϕ defines the magnitude of the uncertainty in ϕ, and γ is a random number between -0.5 and 0.5 (Press *et al.*, 1992). Similarly, random numbers given by $2E_{\delta t}\gamma$ are added to the δt measurements. The resulting depth variations of F_v (Fig. 8) suggest a decreased accuracy when larger E_ϕ and $E_{\delta t}$ values are used. However, even for a poorly constrained data set with uncertainties as large as $\pm 20°$ for ϕ and ± 1.0 s for δt, the minimum F_v values are still found near the true depth of anisotropy, although understandably the significance of the minimum decreases and multiple minima appear with increased noise level.

A uniform block size of $Dx = 0.1°$ is used for all of the preceding synthetic tests. To test the effects of block size on the reliability of the depth-estimation procedure, we perform synthetic tests using a series of Dx values. The results of the tests are shown in Figure 9. When Dx is small (e.g., 0.05°), the number of blocks having two or more measurements is small, leading to an unstable F_v depth variation and large uncertainties. On the other hand, when Dx is too large (e.g., 0.4° or greater for the synthetic parameters), the measurements inside each of the blocks may be spatially inconsistent (especially for continuously varying parameters, such as those used in the synthetic tests), leading to a broadened F_v curve and reduced peak-to-peak amplitude. For slower-varying splitting parameters, a larger Dx can result in more stable results.

Testing Using Seismic Data Recorded on the Ethiopian Plateau

To further test the procedure, we processed all the available broadband seismic data recorded on the Ethiopian Plateau using a well-tested SWS analysis and ranking procedure (Liu *et al.*, 2008; Liu, 2009; Gao *et al.*, 2010). A total of 448 pairs of reliable (quality A or B, see Liu *et al.*, 2008 for ranking criteria) measurements from 52 portable or permanent seismic stations were obtained (Fig. 10). Those measurements show significant spatial but insignificant azimuthal variations, suggesting that seismic anisotropy observed on the Ethiopian Plateau is caused by a single anisotropic layer with horizontal axis of symmetry and spatially varying splitting parameters.

When the depth-estimation procedure is applied to the data set, the resulting F_v curves show a clear minimum at about 300 km, suggesting an asthenospheric origin of the observed anisotropy (Fig. 11). Note that the resulting depth is the same as that of Gao *et al.* (2010), in which linear rather than circular STDs for ϕ are used, due to the high similarity of

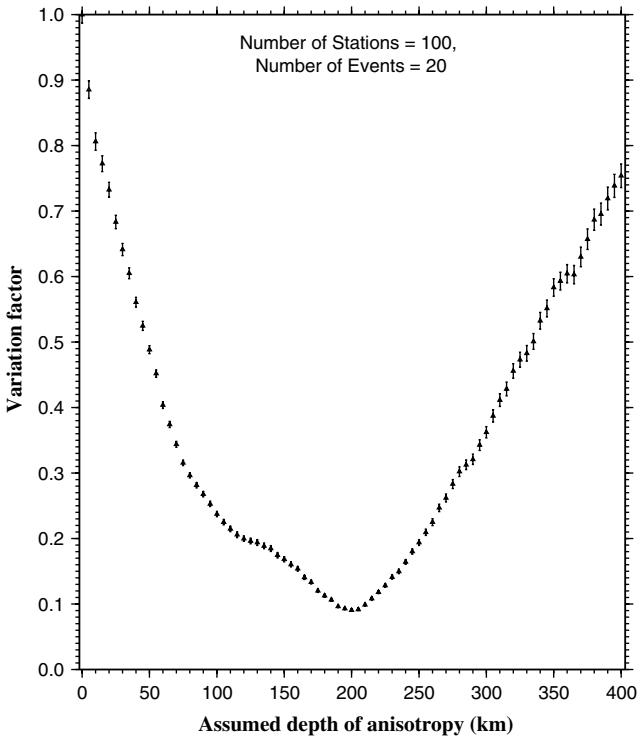

Figure 4. Variation of the spatial variation factor (F_v) as a function of assumed depth of anisotropy computed using the 20 events shown in Figure 2 and the 100 stations shown in Figure 3.

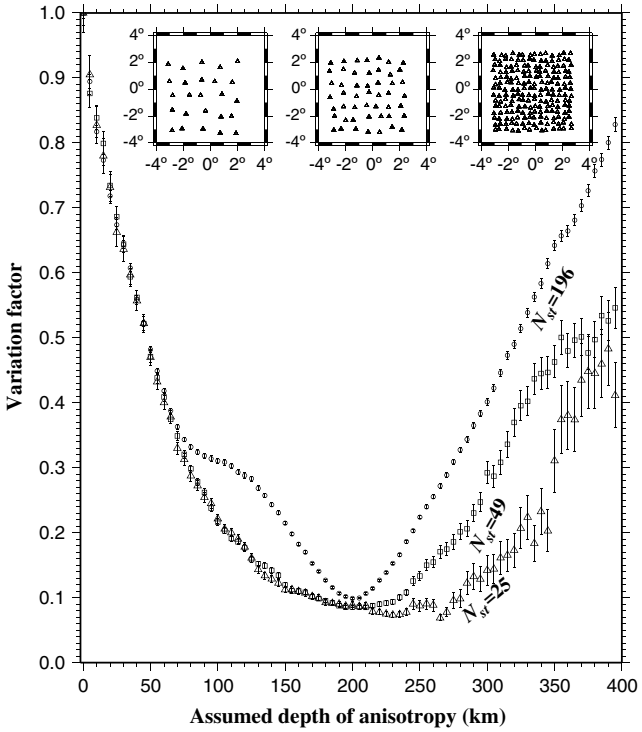

Figure 6. Same as in Figure 4 except for the number of stations (labeled as N_{st} in the figure) used in generating the synthetic data set. The 20 events shown in Figure 2 are used. The insets show the distribution of the stations for N_{st} = 25, 49, and 196, respectively.

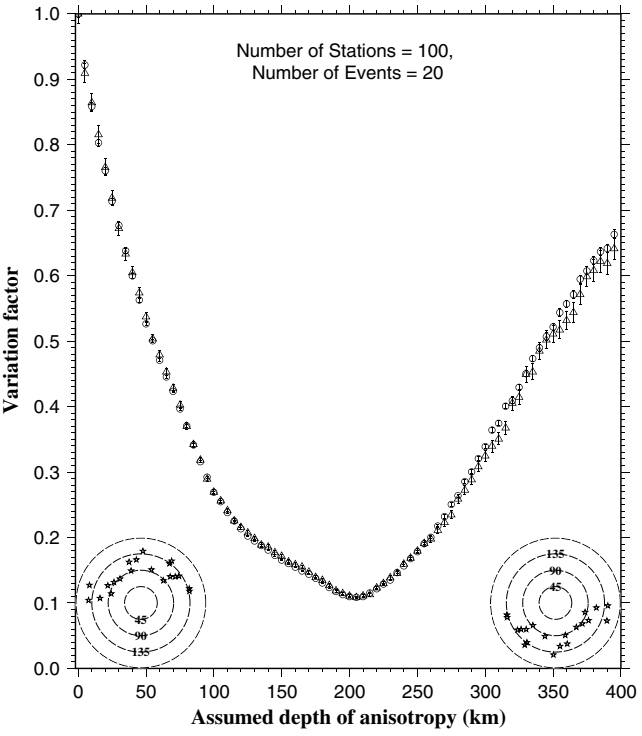

Figure 5. Same as in Figure 4 but for events from the south (circles) and north (triangles). The insets show the distribution of the events.

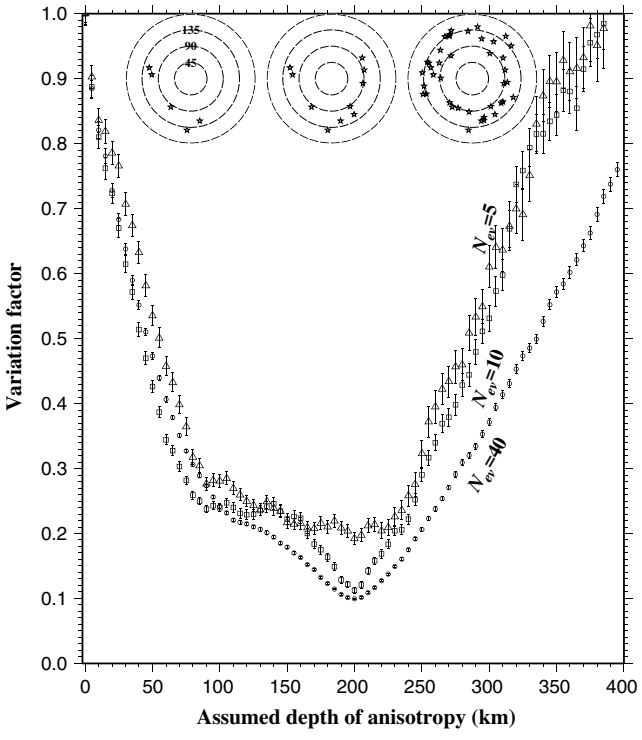

Figure 7. Depth variations of F_v from different numbers of events (labeled as N_{ev} in the figure) used in generating the synthetic data set. The 100 stations shown in Figure 3 are used. The insets show the distribution of the events for N_{ev} = 5, 10, and 40, respectively.

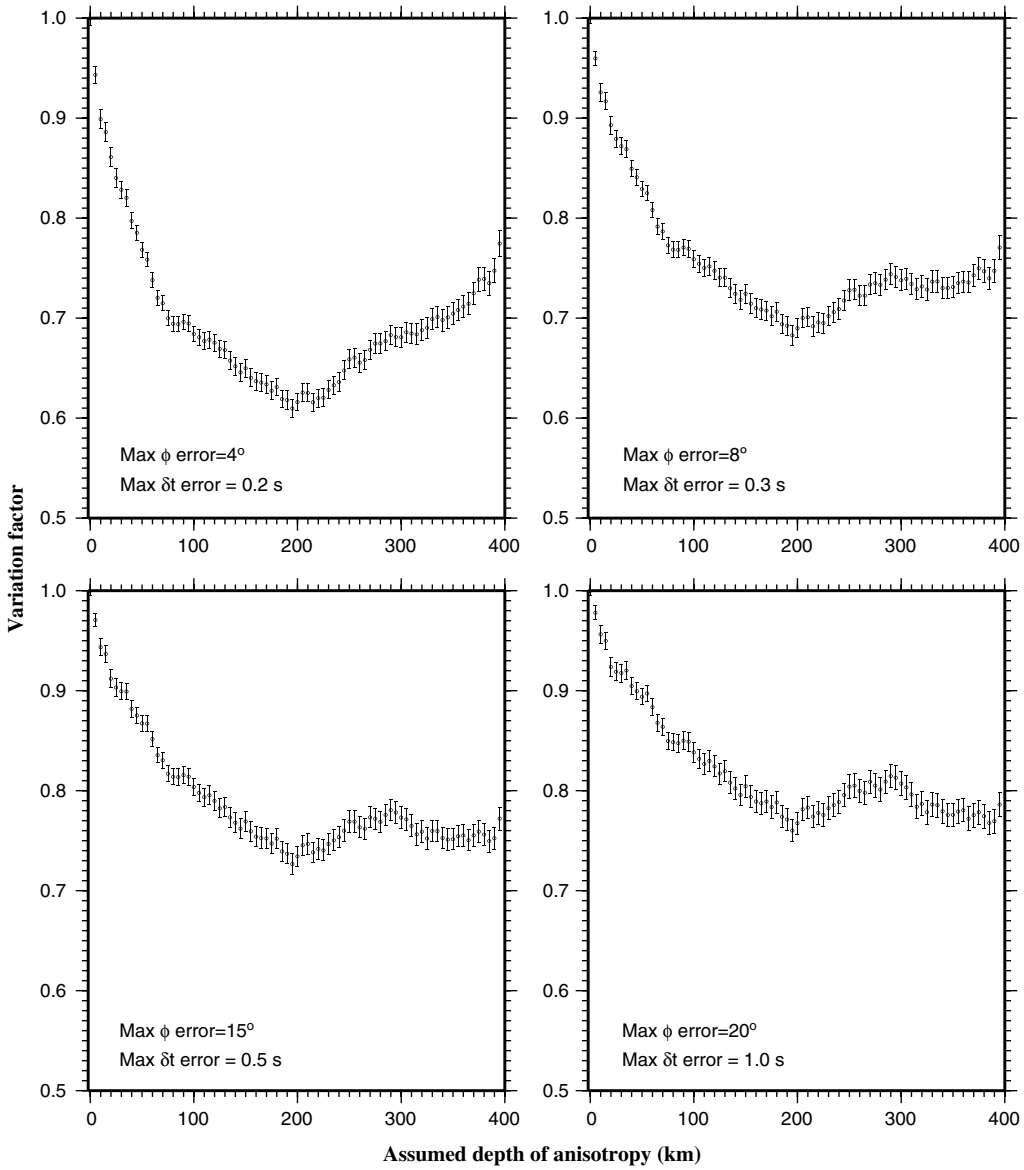

Figure 8. Resulting depth variations of F_v using different noise levels, which are shown in each of the plots as the maximum errors for ϕ and δt.

the ϕ measurements in virtually all of the blocks. Details about the data analysis procedure, comparisons of those results with previous results, and the geodynamic implications of the observations can be found in Gao *et al.* (2010).

Discussion and Conclusions

The tests presented in this article demonstrate that spatial coherency of shear-wave splitting parameters can be used to estimate the depth of anisotropy responsible for observed shear-wave splitting. When the degree of anisotropy (or its vertical distribution) is known, the resultant depth can be used to estimate the (tectonically more significant) depths to the top and bottom of the anisotropic layer.

The success of using the procedure to estimate the depth is dependent on a number of factors. First, a well-determined data set of individual (rather than station-averaged) splitting parameters measured at a sufficient number of stations and from multiple events with adequate azimuthal coverage is required. Results of the synthetic tests (Figs. 5–7) suggest that a more reliably determined depth can be obtained using data from greater numbers of stations and events that are from a broader back-azimuthal range. In addition, the stations must be close enough (relative to the depth of the anisotropic layer) so that the first Fresnel zones from different ray paths partially or entirely overlap. Based on the typical angle of incidence of the *XKS* waves, the overlapping can be achieved if the station spacing is smaller than half of the depth of the anisotropic layer.

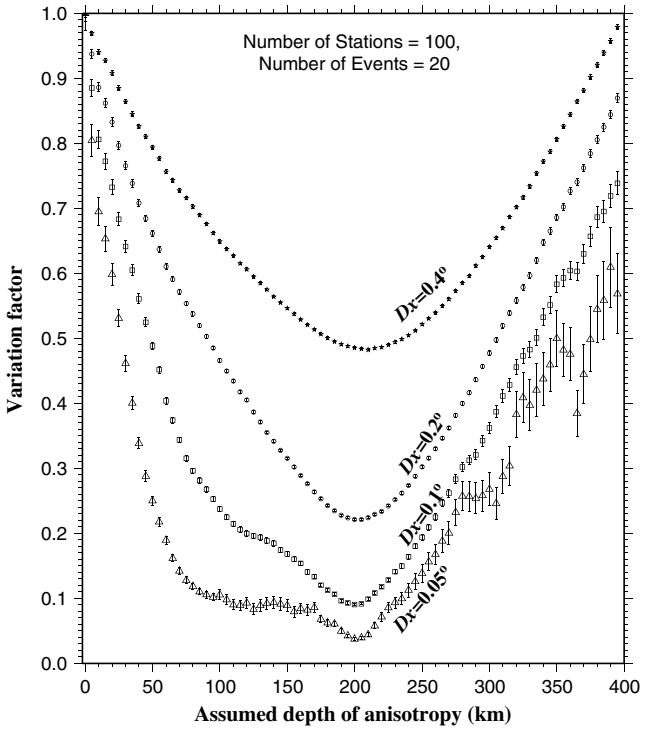

Figure 9. Same as in Figure 4 but for different block dimensions.

The second factor is that there must be significant but smooth spatial variations in the splitting parameters, such as those observed on the Ethiopian Plateau (Fig. 10). Obviously, F_v will be nearly identical for all the assumed depths if there is little spatial variation in the splitting parameters. On the other hand, sharp lateral variations of anisotropy properties lead to unstable splitting parameters in the vicinity of the boundary as revealed by synthetic studies (e.g., Alsina and Snieder, 1995) and thus might contaminate the F_v values.

Third, the source of anisotropy must be in a single layer with a horizontal axis of symmetry. Complex anisotropy, such as multiple layers and/or dipping axes, leads to azimuthal (and thus apparent ray-piercing point location) dependence in the observed splitting parameters (e.g., Silver and Savage, 1994). Including such apparent spatial variations in the depth-estimation procedure will lead to erroneous results. Therefore, it is critical to confidently eliminate the possibility of complex anisotropy before the procedure can be applied to a data set. Plotting the splitting parameters against the back-azimuth of the events and visually checking systematic azimuthal variations are effective ways to identify complex anisotropy. If splitting parameters from two horizontal layers can be isolated using the approach of Silver and Savage (1994), the depth-estimation approach can be applied to the splitting parameters for each of the layers separately to obtain independent depth estimates for the upper and lower layers.

Finally, the depth of the anisotropic layer should be approximately a constant beneath the area in which the depth-estimation procedure is applied. For an area with spatially varying depth, multiple minima can be observed on the F_v variation curve, leading to ambiguities. On the other hand, if the dimension of the area is significantly greater than that of the predicted first Fresnel zone, the ambiguity can be reduced by dividing the area into subareas and performing the depth estimation separately. This process will likely result in tectonically significant spatial distribution of the depth of the anisotropic layer. If this approach is applied to data covering large areas, long-lasting debates about whether observed anisotropy is associated with flow in the asthenosphere (e.g., Vinnik *et al.*, 1992; Gao *et al.*, 1994) or with

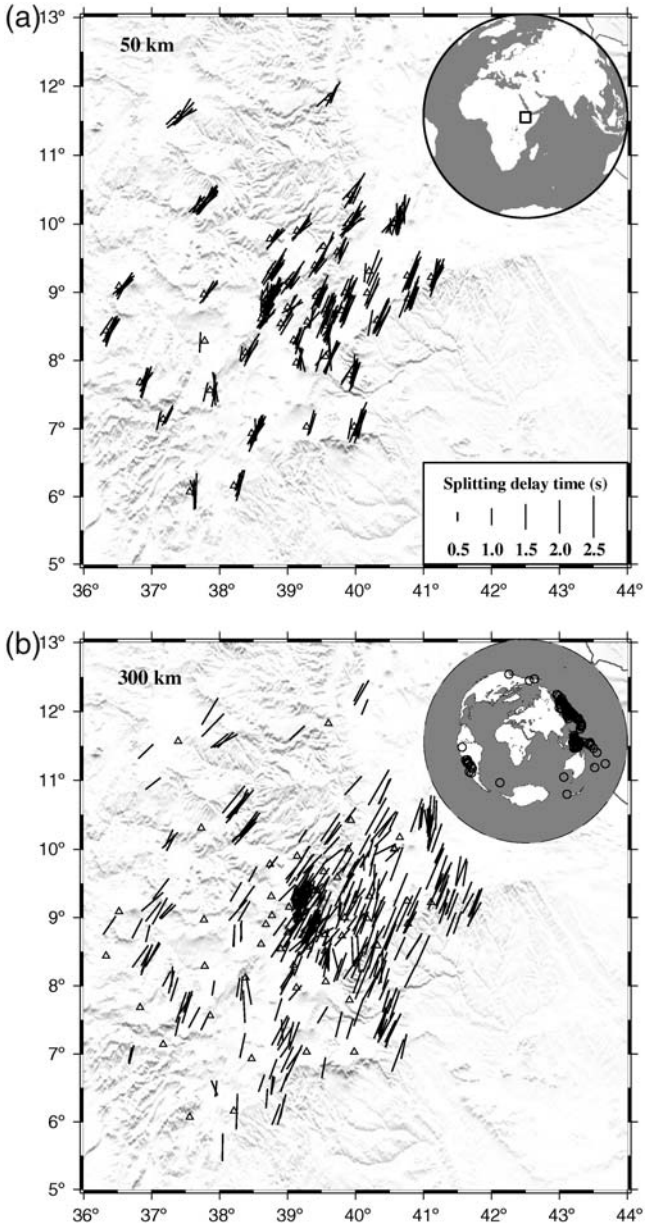

Figure 10. *XKS*-splitting measurements on the Ethiopian Plateau plotted above the ray-piercing points (a) at 50 km and (b) 300 km. Triangles represent seismic stations. The inset map in the upper plot indicates the location of the study area (square), and that in the lower plot shows events (circles) used to produce the SWS measurements (Gao *et al.*, 2010).

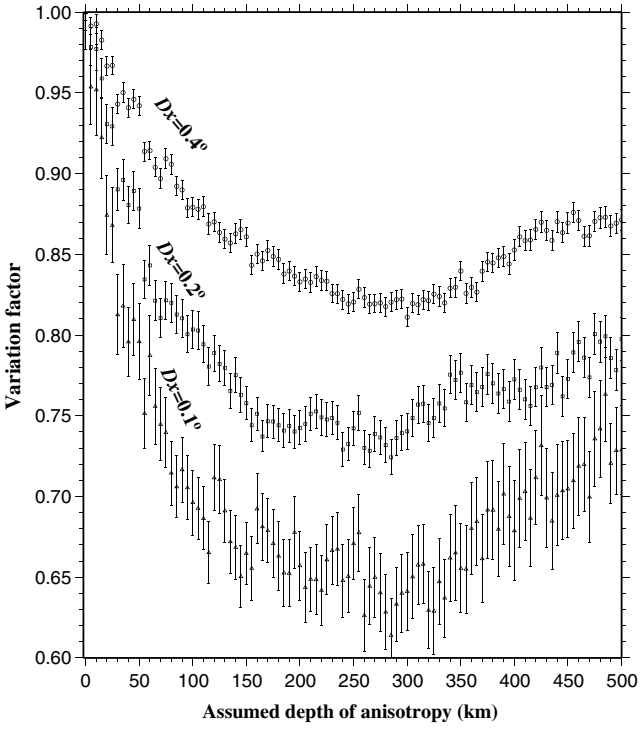

Figure 11. Resulting depth variations of F_v for the Ethiopian Plateau using three different block sizes.

vertically coherent deformation in the lithosphere (e.g., Silver, 1996; Silver *et al.*, 2001) can hopefully be resolved.

Data and Resources

Seismograms recorded in Ethiopia that were used in the study were obtained from the Incorporated Research Institutions for Seismology (IRIS) Data Management Center. Figures were produced by the Generic Mapping Tools (Wessel and Smith, 1991). The *ran4* FORTRAN subroutine from Press *et al.* (1992) was used to generate random values used in this article.

Acknowledgments

We thank Cleat Zeiler, Martha Savage, and an anonymous reviewer for constructive reviews. The study was supported by U.S. National Science Foundation grants EAR-0739015, EAR-0911346, and EAR-0952064. This article is Missouri University of Science and Technology Geology and Geophysics contribution 28.

References

Alsina, D., and R. Snieder (1995). Small-scale sublithospheric continental mantle deformation: Constraints from *SKS* splitting observations, *Geophys. J. Int.* **123,** 431–448.

Chevrot, S. (2006). Finite-frequency vectorial tomography: A new method for high-resolution imaging of upper mantle anisotropy, *Geophys. J. Int.* **165,** 641–657.

Davis, J. C. (2002). *Statistics and Data Analysis in Geology*, Third Ed., John Wiley & Sons, New York, 656 pp.

Favier, N., and S. Chevrot (2003). Sensitivity kernels for shear wave splitting in transverse isotropic media, *Geophys. J. Int.* **153,** 213–228.

Fisher, N. I. (1993). *Statistical Analysis of Circular Data*, Cambridge University Press, London, 296 pp.

Gao, S., P. M. Davis, H. Liu, P. D. Slack, Y. A. Zorin, V. V. Mordvinova, V. M. Kozhevnikov, and R. P. Meyer (1994). Seismic anisotropy and mantle flow beneath the Baikal rift zone, *Nature* **371,** 149–151.

Gao, S. S., K. H. Liu, and M. G. Abdelsalam (2010). Seismic anisotropy beneath the Afar Depression and adjacent areas: Implications for mantle flow, *J. Geophys. Res.* **115,** no. B12330, doi 10.1029/2009JB007141.

Gerst, A., and M. K. Savage (2004). Seismic anisotropy beneath Ruapehu volcano: A possible eruption forecasting tool, *Science* **306,** 1543–1547.

Kennett, B. L. N., and E. R. Engdahl (1991). Traveltimes for global earthquake location and phase identification, *Geophys. J. Int.* **105,** 429–465.

Liu, K. H. (2009). NA-SWS-1.1: A uniform database of teleseismic shear-wave splitting measurements for North America, G^3 **10,** Q05011, doi 10.1029/2009GC002440.

Liu, K. H., S. S. Gao, Y. Gao, and J. Wu (2008). Shear-wave splitting and mantle flow associated with the deflected Pacific slab beneath northeast Asia, *J. Geophys. Res.* **113,** no. B01305, doi 10.1029/2007JB005178.

Press, W. H., S. A. Teukolsky, W. T. Vetterling, and B. P. Flannery (1992). *Numerical Recipes in FORTRAN*, Second Ed., Cambridge University Press, Cambridge, Massachusetts, 1486 pp.

Savage, M. K. (1999). Seismic anisotropy and mantle deformation: What have we learned from shear wave splitting? *Rev. Geophys.* **37,** 65–106.

Silver, P. G. (1996). Seismic anisotropy beneath the continents—Probing the depths of geology, *Annu. Rev. Earth Planet Sci.* **24,** 385–432.

Silver, P. G., and M. K. Savage (1994). The interpretation of shear-wave splitting parameters in the presence of two anisotropic layers, *Geophys. J. Int.* **119,** 949–963.

Silver, P. G., S. S. Gao, and K. H. Liu (2001). Mantle deformation beneath southern Africa, *Geophys. Res. Lett.* **28,** 2493–2496.

Vecsey, L., J. Plomerova, and V. Babuska (2008). Shear-wave splitting measurements—Problems and solutions, *Tectonophysics* **426,** 178–196.

Vinnik, L. P., L. I. Makeyeva, A. Milev, and A. Y. Usenko (1992). Global patterns of azimuthal anisotropy and deformations in the continental mantle, *Geophys. J. Int.* **111,** 433–447.

Wessel, P., and W. H. F. Smith (1991). Free software helps map and display data, *Eos Trans. AGU* **72,** 441, 445–446.

Wustefeld, A., G. Bokelmann, G. Barruol, and J.-P. Montagner (2009). Identifying global seismic anisotropy patterns by correlating shear-wave splitting and surface-wave data, *Phys. Earth Planet. In.* **176,** 198–212.

Department of Geological Sciences and Engineering
Missouri University of Science and Technology
Rolla, Missouri 65409
liukh@mst.edu
sgao@mst.edu

Manuscript received 27 September 2010